JACS
JOURNAL OF THE AMERICAN CHEMICAL SOCIETY
Article
pubs.acs.org/JACS

Si_3AlP: A New Promising Material for Solar Cell Absorber

Ji-Hui Yang,[†] Yingteng Zhai,[†] Hengrui Liu,[†] Hongjun Xiang,*[,†] Xingao Gong,*[,†] and Su-Huai Wei[‡]

[†]Key Laboratory of Computational Physical Sciences (Ministry of Education), State Key Laboratory of Surface Physics and Department of Physics, Fudan University, Shanghai 200433, P. R. China

[‡]National Renewable Energy Laboratory, Golden, Colorado 80401, United States

Supporting Information

ABSTRACT: First-principles calculations were performed to study the structural and optoelectronic properties of the newly synthesized nonisovalent and lattice-matched $(Si_2)_{0.6}(AlP)_{0.4}$ alloy (Watkins, T.; et al. *J. Am. Chem. Soc.* **2011**, *133*, 16212). We found that the most stable structure of Si_3AlP is a superlattice along the ⟨111⟩ direction with separated AlP and Si layers, which has a similar optical absorption spectrum to silicon. The ordered $C1c1$-Si_3AlP is found to be the most stable one among all structures with a basic unit of one P atom surrounded by three Si atoms and one Al atom, in agreement with experimental suggestions.[1] We predict that $C1c1$-Si_3AlP has good optical properties, i.e., it has a larger fundamental band gap and a smaller direct band gap than Si; thus, it has much higher absorption in the visible light region. The calculated properties of Si_3AlP suggest that it is a promising candidate for improving the performance of the existing Si-based solar cells. The understanding on the stability and band structure engineering obtained in this study is general and can be applied for future study of other nonisovalent and lattice-matched semiconductor alloys.

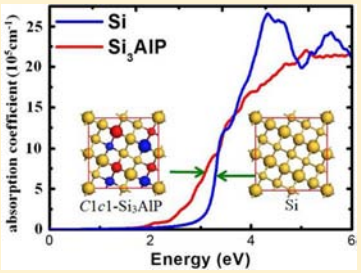

INTRODUCTION

Recently, significant efforts have been devoted to search new or improve existing photovoltaic materials. Among all the existing solar cell technologies, first-generation crystalline silicon-based solar cells are still one of the most important solar cell materials in terms of energy conversion efficiency and utilization. It has reached an efficiency of more than 23% and has a market share of over 80% in the world photovoltaic industry.[2] However, further development of Si-based solar cells is limited by the intrinsic material properties of Si, i.e., it has an indirect band gap and a relatively low band gap energy (~1.1 eV). For developing new solar cell absorber with optimal performance, it would be desirable to find a new material based on Si, which has a more direct and relatively higher band gap to improve its solar conversion efficiency.

For conventional semiconductors, when group IV elements mutate into its corresponding III−V and II−VI compounds, both the band gap and the directness of the band gap (the energy difference between the fundamental band gap and the lowest direct band gap) increases with increased ionicity. For example, for Ge, GaAs, and ZnSe, Ge has an indirect band gap of 0.7 eV, whereas GaAs and ZnSe have direct band gaps of 1.5 and 2.8 eV, respectively. Therefore, to modify the band structure of Si for solar absorbers, it will be natural to try alloying Si with its mutated III−V or II−VI semiconductors such as AlP or MgS. These nonisovalent $(IV_2)_{1-x}(III-V)_x$ alloys are expected to have a wide range of band gaps, and more importantly, they are lattice matched, which can provide us great flexibilities to tune the band gap for specific applications such as tandem solar cells. However, only a few of these alloys have been studied and applied in practice. One of the examples is BNC_2, which is an alloy of diamond and cubic BN. This mixed alloy is chemically more stable than C but also with a super hardness comparable to that of diamond.[3−5] Some studies have also been done on $(Ge_2)_x(GaAs)_{1-x}$[6−8] alloy for producing a 1 eV direct band gap absorber lattice matched to GaAs. The main problem for these nonisovalent $(IV_2)_{1-x}(III-V)_x$ alloys is that under normal growth conditions these alloys tend to phase separate due to large chemical mismatch, thus preventing group IV semiconductors from forming homogeneous alloys with III−V semiconductors. It is, therefore, very exciting to notice that very recently Si_3AlP, an alloy between Si and AlP, has been successfully synthesized by Watkins et al.[1] using gas source (GS) MBE. This material is lattice matched to Si and could have potential to significantly improve the performance of crystalline Si solar cells. In their paper, several structures are proposed for this kind of materials based on the experimental work. They calculated the band structures for some of the structures,[9] but no detailed theoretical analysis was carried out. Therefore, so far, the atomic configurations, structural stabilities, and optoelectronic properties of this important nonisovalent semiconductor alloy are not fully investigated.

CALCULATION METHODS

In this article, we investigated the stability and optoelectronic properties of Si_3AlP and its suitability as a new material for improving the performance of the existing Si-based solar cells by performing first-principles density functional theory (DFT) calculations.[10,11] The local density approximation (LDA) is used to relax the structure parameters as implemented in the VASP code. The electron and core interactions

Received: April 23, 2012
Published: July 9, 2012

   dx.doi.org/10.1021/ja303892a | *J. Am. Chem. Soc.* 2012, 134, 12653−12657

are included using the frozen-core projected augmented wave (PAW) approach.[12] The cutoff kinetic energy for the plane-wave basis wave functions is chosen to be 400 eV for all calculations. The Brillouin zone (BZ) integration was carried out using 8 × 8 × 6 gamma-centered Monkhorst–Pack *k*-point meshes[13] for the 10-atom Si_3AlP primitive cell and equivalent *k* points for the other cells. All lattice vectors and atomic positions are fully relaxed until the quantum mechanical forces became less than 0.01 eV/Å. For the optical spectrum calculations, we used the DFT-LDA code to calculate the imaginary dielectric functions for qualitative comparisons. Then we performed more accurate calculations for *C*1*c*1-Si_3AlP using Bethe–Salpeter equation (BSE) method implemented in the Yambo code, where the LDA band error is corrected using the GW approach.[14] We find that the relative changes of the band structure between Si and Si_3AlP is not sensitive to the GW correction.

RESULTS AND DISCUSSION

Structural Analysis. An experimental study by Watkins et al.[1] suggested that the conventional 20-atom Si_3AlP cell consists of four basic units of $[AlPSi_3]$, which can be seen as a $(5/2)^{1/2}a \times (5/2)^{1/2}a \times a$ Si supercell (a is the lattice constant of the conventional 8-atom Si cell). In this cell, P atoms are assumed to arrange in a way identical to the C atoms in the Si_4C structure,[15,16] forming a square lattice with each column separated by a chess Knight move from its neighbors (Figure 2). However, the energetic stability for such Si_3AlP structures has not been either theoretically analyzed or experimentally confirmed.

Here we sampled all 10-atom structures with the diamond-like lattice considering both the shapes of the cells and the atomic configurations. Five kinds of cells and 457 non-equivalent structures are obtained and fully relaxed. We found that the most stable structure is a superlattice along the ⟨111⟩ direction with separated AlP and Si layers, which adopts a *R*3*m* symmetry as shown in Figure 1. There are 11 Si–Si bonds, 7 Al–P bonds, 1 Si–Al bond, and 1 Si–P bond. No Al–Al bonds or P–P bonds are formed in the superlattice structure. Larger superlattices are tested, and phase separation between Si and AlP regions is confirmed. The superlattice structure is most energetically stable because it maximizes Si–Si and Al–P bonds and minimizes the Al–Al and P–P bonds. As the numbers of Si–Si bonds and Al–P bonds decrease and the numbers of Si–Al bonds and Si–P bonds increase, the energies of these Si_3AlP structures increase in general. Forty seven other structures are found with smaller energies than that of the experimental *C*1*c*1 (noted as *Cc* for short hereafter) structure.

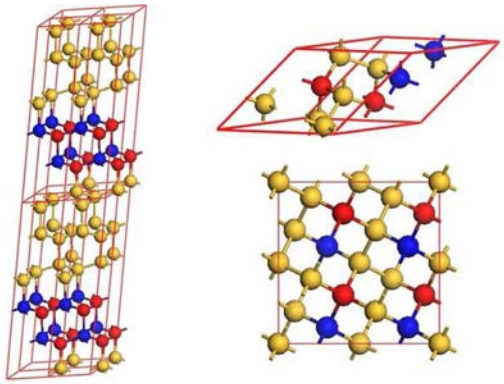

Figure 1. (a) Most stable structure of 10-atom Si_3AlP is shown as a superlattice with a *R*3*m* symmetry (2 × 2 × 2 supecell of the unit cell is given to show their local coordinated atoms). (b) Primitive cell and conventional cell of *C*1*c*1 structure. Red balls are P, blue balls are Al, and yellow balls are Si.

Under experimental growth conditions,[1] each P atom is surrounded by one Al and three Si atoms and every Al atom is surrounded by 3 Si and 1 P (referred to as the $[AlPSi_3]$ motif). Thereafter, we will focus on the structures which keep such motifs. We find that the experimentally proposed *Cc* structure maximizes the Si–Al and Si–P bonds while keeping Al–P bonds: It has 6 Si–Si bonds, 2 Al–P bonds, 6 Si–P bonds, and 6 Si–Al bonds (Figure 1). The Al–P bonds are favorable because this can be treated as a $P_{Si} + Al_{Si}$ donor–acceptor pair, bound by Coulomb attraction.

Besides the *Cc* structure, 12 structures with the 10-atom cell are found to have the same first-neighbor local chemical environment as the *Cc* structure. We further searched the 20-atom cells, and 7021 nonequivalent structures are obtained with 17 different shapes. There were 1353 structures found to be *Cc*-like structures. We also randomly generate some *Cc*-like structures in a 40-atom cell with the same local motif (Supporting Information). Among all of them, the *Cc* structure is found to be the most stable one. We also calculated the phonon spectrum of the *Cc* structure and found no imaginary modes (see Supporting Information), suggesting the stability of this structure.

To study how the different arrangements of the $[AlPSi_3]$ motif affect the structural stabilities and optical and electronic properties, we selected some *Cc*-like structures in the experimentally proposed 20-atom cell by considering the cases where four P atoms in the supercell are fixed as in the *Cc* structure, as shown in Figure 2. Except for the *Cc* structure, the other *Cc*-like structures all adopt a *P*1 symmetry after relaxation. To see why the *Cc* structure is the most stable one among all structures with $[AlPSi_3]$ motifs, we calculate the strain relaxation energy and the electrostatic Coulomb energy. When we estimate the electrostatic Coulomb energy, we set the charges of Si, Al, and P to be 0, +1, and −1, respectively. This choice for the charges is supported by the Bader charge analysis on the *Cc* structure (Supporting Information). We found that the *Cc* structure has the largest relaxation energy and the lowest

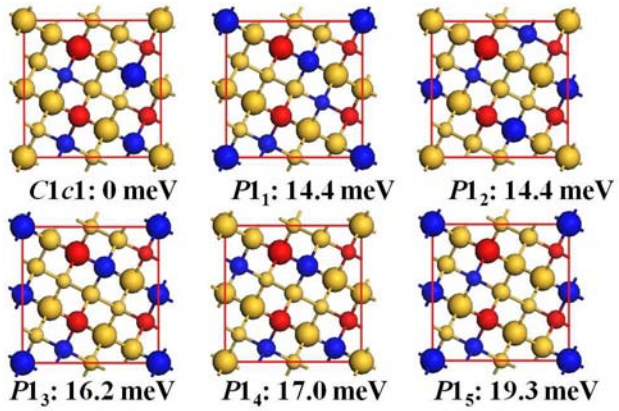

Figure 2. Six different $[AlPSi_3]$ motif arrangements in a 20-atom cell are shown from the top of the (001) surface, labeled by their symmetry group and the energy difference per atom relative to *Cc*-Si_3AlP. Atoms in the upper layers are drawn with larger sizes, and four layers are shown. We use the same colors as Figure 1.

dx.doi.org/10.1021/ja303892a | J. Am. Chem. Soc. 2012, 134, 12653–12657

Coulomb energy, as shown in Table 1, and thus is most energetically favorable among these *Cc*-like structures. The relative energies of the other selected arrangements are also given. They all have a higher energy than *Cc* structure due either to their small relaxation energy or to their large Coulomb energy caused by their second or third neighbors. We also found that formation of Al−Al bonds is not energetically favorable (we constructed a structure containing one Al−Al bond while keeping P atoms fixed as in the 20-atom *Cc* structure for our test (Supporting Information)). It shows that formation of one Al−Al bond can increase the total energy by about 0.59 eV in the cell, which is much larger than the room-temperature kT (~0.034 eV). This suggests that at room temperature the possibility of forming an Al−Al bond should be very small and can be explained by the large Coulomb repulsion energy between Al atoms and the weak Al−Al bond.

Table 1. Energy Analysis of Different *Cc*-Like Structures: The Strain Relaxation Energy Is Defined As the Energy Gain after Structural Optimization[a]

structure	strain relaxation energy (eV/atom)	Madelung energy in ideal lattice (eV/atom)	Madelung energy after relaxation (eV/atom)
Cc	0.040	−4.75	−4.71
$P1_1$	0.034	−4.57	−4.53
$P1_2$	0.034	−4.57	−4.53
$P1_3$	0.033	−4.60	−4.57
$P1_4$	0.032	−4.63	−4.57
$P1_5$	0.035	−4.42	−4.36

[a]The Madelung energy is the total coulomb energy by considering the net charge of every ion. Here, for estimation, we suppose Al has a net charge of +1, P has a net charge of −1, and Si has a 0 net charge, based on our Bader analysis (Supporting Information). The structures listed are shown in Figure 2.

The calculated lattice mismatch between Si_3AlP and Si is very small, less than 0.6% (Supporting Information), which is consistent with the fact that the experimental lattice constants of Si (5.4306 Å) and AlP (5.4510 Å) are very similar. We also found that due to the lower symmetry, the lattice of the ordered *Cc*-Si_3AlP is slightly distorted after relaxation. The angle between a and b is about 89.66° instead of the ideal value of 90°, in good agreement with prior work.[1] This distortion could be reduced if the alloys become less ordered.

Optical Spectra. We first tested the optical properties of those 10-atom structures which are more energetically favorable than the *Cc* structure. Figure 3 shows the calculated imaginary dielectric functions of Si, the superlattice structure, and the *Cc* structure using LDA. The other 47 structures which have lower energy than the *Cc* structure have optical spectra between *Cc* and superlattice, which are given in the Supporting Information. We find that the *Cc* structure, which is just the structure synthesized by the experiment, has the best optical properties compared to pure Si as it has the best absorption below 3.5 eV, while the superlattice structure has almost the same optical property to pure Si (see Figure 3). This can be understood by the fact that the *Cc* arrangement has maximized the mixture between AlP and Si and thus maximized the band coupling between AlP and Si, leading to its best optical performance, as discussed in the next part. This proves the *Cc* structure is preferred for solar cells.

To get more accurate optical properties, we further calculated the absorption coefficients as a function of energy for *Cc*-Si_3AlP and Si using the GW method, which are shown in Figure 4. The GW plus BSE result of Si agrees very well with the experimental result.[17] From the calculated results, we can see that, relative to the absorption spectrum of Si, *Cc*-Si_3AlP has a much higher absorption in the low-energy region (~2.0 eV), which is caused by its smaller optically active direct band gap than that of Si. The GW+BSE results show that Si_3AlP has a remarkable absorption starting from about 3.0 eV compared to about 3.2 eV in Si, which are close to their respective direct band gaps at the Γ point. However, for Si_3AlP, the increase in the absorption below this energy is also significant due to the alloying-induced/enhanced optical absorption.

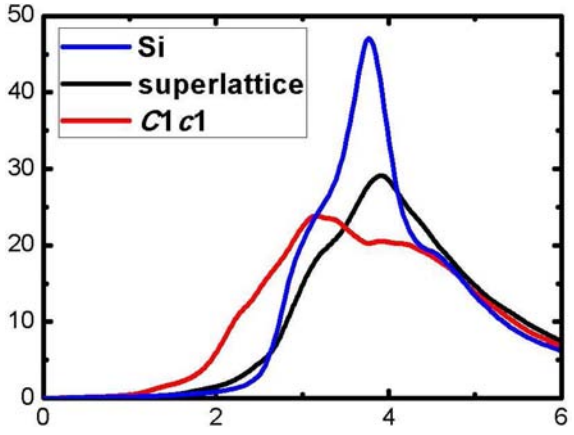

Figure 3. Calculated imaginary dielectric functions versus energy using the LDA method for Si, superlattice structure, and *Cc*-Si_3AlP. Note that this is only to show the superlattice structure is not preferred for improving Si solar cells.

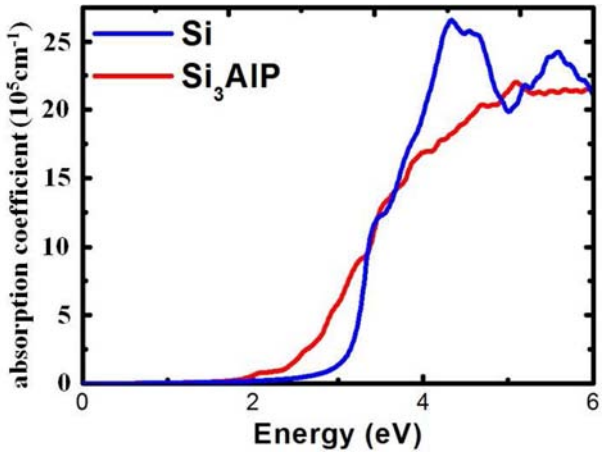

Figure 4. Calculated absorption coefficients for Si and *Cc*-Si_3AlP as a function of energy through the GW plus BSE method.

To study how the different arrangements of the $[AlPSi_3]$ motif affect the optical properties, we also calculated the optical spectra of the other *Cc*-like structures shown in Figure 2 (see Supporting Information). We find that they have almost the same optical spectra as the *Cc* structure. This indicates that the optical properties of these materials are not sensitive to the atomic arrangements in the unit cell, as long as the basic motif is kept, which provides convenience for the synthesis.

Reasons Why Si_3AlP Has Better Optical Properties. To investigate why the *Cc* and *Cc*-like structures have the best optical properties, we calculated the band structure of *Cc*-

dx.doi.org/10.1021/ja303892a | J. Am. Chem. Soc. 2012, 134, 12653−12657

Si_3AlP, which is shown in Figure 5. The valence band maximum (VBM) is at the Γ point, and the conduction band minimum

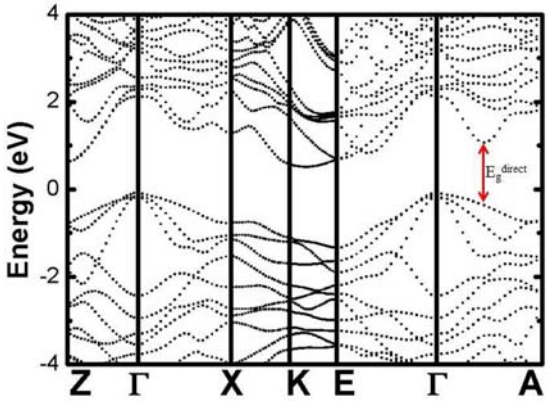

Figure 5. Calculated LDA band structures of *Cc*-Si_3AlP.

(CBM) is at a point along the E−K line. Our LDA calculations find that the indirect band gap of *Cc*-Si_3AlP is 0.16 eV larger than that of Si, so adding AlP to Si increases the fundamental band gap. For *Cc*-Si_3AlP the minimum direct band gap is found at a point along the Γ−A line (Figure 5). The calculated direct band gap at the Γ point for *Cc*-Si_3AlP is 0.33 eV smaller than that of Si at the Γ point; thus, adding AlP to Si reduces the optical band gap. The increase of the indirect fundamental band gap of Si_3AlP than Si is beneficial in increasing the open-circuit voltage, and the decrease of the direct optical band gap is beneficial in increasing the absorption and, thus, the photocurrent of the solar cell. The calculated band structures for other configurations shown in Figure 2 are quite similar to the *Cc* structure (Supporting Information), with variation of the fundamental band gap less than 0.12 eV, indicating that as long as the basic motif is the same the indirect band gap is not sensitive to the atomic arrangements.

The change of the optical band gap can be understood as follows. For the minimum direct band gap along the Γ−A line, the VBM at this *k* point originates from the Si 3p state whereas the CBM is derived from hybridization of Si 3s and 3p states. In pure Si, the transition between the two states is not allowed because they are folded from two different *k* points in the 2-atom Si BZ. However, after AlP is mixed into Si, due to the reduced symmetry, nondiamond potential is introduced to couple different folded states and this transition becomes allowed for Si_3AlP. This explains why *Cc*-Si_3AlP has a much higher absorption in the low-energy region (~2.0 eV) than Si.

For the direct band gap at Γ point, before AlP is introduced, the CBM originates from the Si 3p state. After AlP is mixed, the CBM energy at Γ is expected to initially increase and switch to a more s-like state because the AlP p-like Γ_{15} conduction band state is much higher in energy than the s-like Γ_1 state (Figure 5; electron characters at these special *k* points are given in the Supporting Information for a better understanding).

This, however, contradicts the calculated results, which show the CBM at Γ decreases when AlP is added. This is because in the supercell of Si_3AlP there are states folded to the Γ point and these states will couple with the CBM state at Γ and push the CBM down. These two effects lead to the lowering of the CBM of *Cc*-Si_3AlP than that of Si. A similar case also happens to the VBM state. On one hand, introduction of AlP will lower the VBM state; on the other, coupling to the folded states at the Γ point pushes the VBM upward, Figure 6. Thus, the VBM of *Cc*-Si_3AlP is only slightly lower than that of Si. Taking all of the

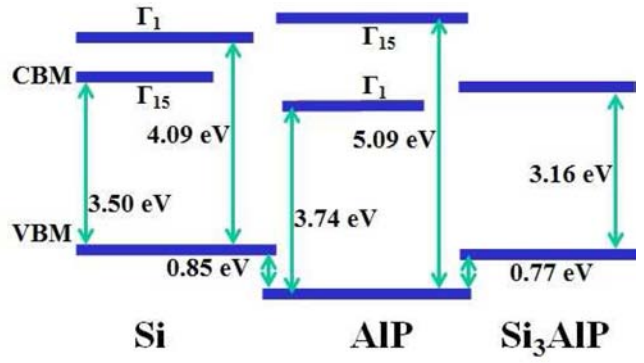

Figure 6. Band alignments at Γ point between Si, AlP, and Si_3AlP. VBM states are aligned through our band offset calculations, while the CBM states are aligned using the experimental band gaps of Si and AlP and GW band gap corrections.

above into account, the optical band gap at the Γ point of *Cc*-Si_3AlP is smaller than that of Si or AlP. This explained why the sharp jump of the *Cc*-Si_3AlP optical spectrum starts at a lower energy than Si, which is beneficial to generate more photocurrent.

CONCLUSION

We systematically studied the structural, electronic, and optical properties of the newly synthesized nonisovalent and lattice-matched $(IV_2)_{1-x}(III-V)_x$ alloy Si_3AlP. *Cc*-Si_3AlP is found to be the most stable structure within the experimentally observed unit cell, but the electronic and optical properties of the alloy are not sensitive to the atomic arrangement in the unit cell as long as the local [Si_3AlP] clusters are maintained. We find that, comparing to Si, Si_3AlP has a larger fundamental band gap and a smaller direct band gap at Γ and thus is more suitable for solar cell absorbers than Si. Therefore, we propose that Si_3AlP could be a strong candidate for photovoltaic applications. Experimental efforts for studying this material for photovoltaic absorber are called for.

ASSOCIATED CONTENT

Supporting Information

Unrelaxed lattice vectors and atomic positions of *Cc* structure, structure with one Al−Al bond in a 20-atom cell, two *Cc*-like 40-atom structures, phonon spectrum of *Cc* structure, Bader analysis of atomic charge in the *Cc* structure, lattice parameters of relaxed structures of Si, AlP and Si_3AlP using LDA functional, calculated imaginary dielectric function of the 10-atom structures that are more energetically stable than the *Cc*-structure, absorption coefficients versus energy for all six *Cc*-like structures, band structures of Si in its 2-atom cell and in 10-atom *Cc*-Si_3AlP cell, electron characters at the special *k* points in the same 10-atom cell for Si and *Cc*-Si3AlP, band structures of the six 20-atom structures, and atom positions and energies of relaxed structures. This material is available free of charge via the Internet at http://pubs.acs.org.

AUTHOR INFORMATION

Corresponding Author

*hxiang@fudan.edu.cn; xggong@fudan.edu.cn

Notes

The authors declare no competing financial interest.

■ ACKNOWLEDGMENTS

The work at Fudan University was partially supported by the Special Funds for Major State Basic Research, National Science Foundation of China (NSFC), International collaboration project, NSFC, Pujiang plan, and Program for Professor of Special Appointment (Eastern Scholar). Computation was performed in the Supercomputer Center of Fudan University. The work at NREL was funded by the U.S Department of Energy (DOE), under Contract No. DE-AC36-08GO28308.

■ REFERENCES

(1) Watkins, T.; Chizmeshya, A. V. G.; Jiang, L.; Smith, D. J.; Beeler, R. T.; Grzybowski, G.; Poweleit, C. D.; Menéndez, J.; Kouvetakis, J. *J. Am. Chem. Soc.* **2011**, *133*, 16212.
(2) Goetzbergera, A.; Heblinga, C.; Schock, H.-W. *Mater. Sci. Eng. R* **2003**, *40*, 1−46.
(3) Zholozenko, V. L.; Andrault, D.; Fiquet, G.; Mezouar, M.; Rubie, D. C. *Appl. Phys. Lett.* **2001**, *78*, 1385.
(4) Chen, S.; Gong, X. G.; Wei, S.-H. *Phys. Rev. Lett.* **2007**, *98*, 015502.
(5) Chen, S.; Gong, X. G.; Wei, S.-H. *Phys. Rev. B* **2008**, *77*, 014113.
(6) Holloway, H.; Davis, L. *Phys. Rev. Lett.* **1984**, *53*, 1510.
(7) McGlinn, T. C.; Klein, M. V.; Romano, L. T.; Greene, J. E. *Phys. Rev. B* **1988**, *38*, 3362.
(8) Norman, A. G.; Olson, J. M.; Geisz, J. F.; Moutinho, H. R.; Mason, A.; Al-Jassim, M. M.; Vernon, S. M. *Appl. Phys. Lett.* **1999**, *74*, 1382.
(9) Watkins, T.; Jiang, L.; Xu, C.; Chizmeshya, A. V. G.; Smith, D. J.; Menéndez, J.; Kouvetakis, J. *Appl. Phys. Lett.* **2012**, *100*, 022101.
(10) Hohenberg, P.; Kohn, W. *Phys. Rev.* **1964**, *136*, B864.
(11) Kohn, W.; Sham, L. J. *Phys. Rev.* **1965**, *140*, A1133.
(12) Kresse, G.; Joubert, D. *Phys. Rev. B* **1999**, *59*, 1758.
(13) Monkhorst, H. J.; Pack, J. D. *Phys. Rev. B* **1976**, *13*, 5188.
(14) Marini, A.; Hogan, C.; Grüning, M.; Varsano, D. *Comput. Phys. Commun.* **2009**, *180*, 1392.
(15) Rücker, H.; Methfessel, M.; Bugiel, E.; Osten, H. J. *Phys. Rev. Lett.* **1994**, *72*, 3578.
(16) Zhang, P.; Crespi, V. H.; Chang, E.; Louie, S. G.; Cohen, M. L. *Phys. Rev. B* **2001**, *64*, 235201.
(17) Lautenschlager, P.; Garriga, M.; Viña, L.; Cardona, M. *Phys. Rev. B* **1987**, *36*, 4821.